Response to Referee 1

We would like to thank the Referee for their thoughtful comments. More detailed responses to each point are outlined below.

COMMENTS TO THE AUTHOR(S): This well-written and well-structured manuscript describes the development, validation and application of an instrument based on incoherent broadband cavity-enhanced absorption spectroscopy (IBBCEAS) for the direct detection and quantification of ozone in the UV-C region (~265 nm). The pulsed instrument (Rapid Ozone Experiment, ROZE) is designed for O3 Eddie covariance measurements from airborne platforms and thus requires high time resolution. The authors give an excellent motivation for their work in the introduction. They briefly review the measurement principle before outlining the instruments operation, where sufficient attention to detail is provided to understand the function of the instrument and how the key objectives in instrument performance were met. The lab characterization of the instrument's performance addresses all relevant aspects. Finally, the first application in airborne operation also shows the quality of the instrument for Eddie covariance measurements in comparison with a more established chemiluminescence (reference) approach. The authors pay sufficient attention to detail, error discussion, and relevant critical measurement parameters. The manuscript is basically publishable in its current form, however subject to some improvement and amendments concerning more explanations as outlined below.

1. L49: The UV region has the drawback that in this region many other trace species also have significant absorption bands and this puts substantial constraints on the selectivity of the method in that region. See also comment below (L216-220).

2. L70-74: The use of an optical filter simplifies the approach and is adequate because the spectrum is unstructured and the absorption has not much or very little "fingerprint character". However, it also illustrates the low selectivity for ozone in this region (see L216-220).

   Points 1 and 2 will be addressed in response to question 11 below.

3. L101: The divergence of the LED is quite large – the surface area of LED is also large 1x1 mm^2 (extended light source). Light collection at a distance of 79 mm with a 1" diameter optic causes substantial light loss. Using a beam expander in reverse increases the divergence after partial collimation again by a factor of 2. Can the authors give an estimate what fraction of the overall emission from the LED is actually being imaged onto the cavity – in other words, what is the light collection efficiency for the LED?

   We estimate the LED collection efficiency to be at minimum ~1–2%. Additionally, as the mirrors are 99.7% reflective, only ~0.3% of the remaining intensity enters the cavity. Although light losses are large, the PMT detector is not signal-limited. We empirically found that the 79 mm focal length lens and beam expander combination achieved the most effective collimation and optimized the optical pathlength.

4. L103: "…direct the beam 180° into the cell." This sounds strange. Please rephrase or at least refer to Figure 3 here.

1

The text on L104 has been altered as: *…two mirrors (Thorlabs NB1-K04) turn the beam 180° into the cell (see Figure 3)…*

5. L105-114 (section 3.1.2): There is no mention of a purge system. Were the cavity mirrors purged? If not – why not? There is also no mention of an aerosol filter in the inlet at this point, but later the authors point this out (since scattering in the UV is substantial). This section would benefit from mentioning these elements explicitly here.

    Purging the cavity mirrors was not found to be necessary to keep them clean. Instead we affixed a filter to the cell inlet port to exclude dust and other particles > 2µm. We have edited and moved the appropriate text from Section 3.2 to Section 3.1.2:

    L112: *A 2-micron pleated mesh filter (Swagelock) affixes to the sample cell inlet port to exclude dust and other particles from affecting the mirror reflectivity, as the mirrors are not independently purged.*

    The aerosol filter is not a permanent fixture in the instrument; it was added to the flow system as an extra precaution in anticipation of the high aerosol load in smoke plumes and is therefore described in Section 5, "Field demonstration". Although we were still able to achieve an 11 SLM flow rate and acquire eddy covariance O_3 flux measurements, removing the particle filter or replacing it with a higher throughput filter would enable a faster response time for dedicated O_3 flux measurements in a cleaner environment. The text in Section 5 has been modified to read:

    L212: *The instrument operated as described above, with the addition of an inline particle filter (Balston 9922-05-DQ) to protect the cavity mirrors from fine particulates in the targeted smoke plumes. Although more aggressive filtering comes at the cost of reduced flow rates and thus lowers the instrument response time, O_3 deposition measurements were not a primary objective of FIREX-AQ.*

6. L125/126: At this point I was wondering whether there was a flow controller? The flow seems to be only controlled by pump power? How accurate is the flow and how does it vary with pressure variation? (Relevant for aircraft measurements on the ascent and descent). What are the three flows according to the 3 flow speed adjustments?

    There is no flow controller and thus the flow varies with pressure: for a fixed ambient pressure, higher sample flows result in lower pressures within the sample cell. The flow also changes in flight with aircraft speed. The pressure gauge provides accurate (± 0.2%) pressure readings for calculating the O_3 mixing ratio. The flow meter is accurate to within ± 3%, but this component does not go into calculation of the O_3 mixing ratio.

    The three flows are user-adjustable and were configured to be roughly 2, 5, and 11 SLM during the FIREX-AQ deployment. These have been noted in the text on L128.

7. L145: Here it would be nice to explicitly learn what on- and off-times a 90% duty cycle refers to? Are there are delay times. Inherently pulsed IBBCEAS is not commonly applied and in the literature the large majority of instruments is indeed continuous wave. Pulsed IBBCEAS can in principle be biased by offsets depending on the measurement timing, which in turn may lead to systematic deviations in the measured absorption signal (see e.g. Keary & Ruth, Opt.

2

Express, 2019). The authors may want to make an argument that these offsets are not observed here based on the electronics' timing. See also comment on Fig. 1 below.

The duration of the ON and OFF LED pulses (900 µs and 100 µs respectively) has been added to the text (L143). Due to the fast digitization rate of our ADC unit (100x faster than the LED modulation rate), we have configured the data acquisition to minimize any delay in gated signal averaging, as it was not necessary to introduce any delay for measurement purposes.

8. L182/183: "…*and differential scatter or absorption due to non-uniform flow within the sample cell at high flow rates.*" As in the comment above, more on flow variation and or flow control would be helpful. The instrument might benefit from a pressure controlling flow controller.

See response to question 6 above.

9. L205: "*During this experiment, the pump maintained a sample flow rate of 18 SLM.*" Why was this not done at a lower mass flow of 11 SLM relevant for the airborne measurements with particle filter?

We performed the pulsed valve experiment to determine the maximum achievable instrument response time using only the permanent 2 µm mesh filter. As described in response to question 5 above, the Balston particle filter could be removed or replaced with a higher throughput filter when using the instrument for dedicated eddy covariance flux observations in environments where we do not expect such a high burden of fine particulates.

10. L206: I am a bit confused here: Please explain "3e fold flush rate". Also compare with caption of Fig 6 which says 1/3e is 9.5 Hz. The 3e-folding time is 150 ms (6.6 Hz)? A few more words would help.

The exponential fit yields a decay constant, or *e*-folding time of tau = 50 ms. The decay is exponential, so the time for O_3 to decay to $1/3e$ (~12%) of its initial concentration is ~105 ms, or 9.5 Hz. The text on L205 has been clarified as: *The time to flush the cell to 1/3e of its initial contents thus corresponds to a flush rate of 9.5 Hz.*

11. L216-221: "*In fresh, concentrated smoke plumes, UV active species such as SO2 and aromatic hydrocarbons can give rise to positive artifacts in the O3 absorption measurement (Birks, 2015). … However, such UV-active absorbers are generally not abundant enough in the background atmosphere to be of concern.*" This paragraph, which is a consequence of the low selectivity of the method for Ozone in the UV region, leaves a lot of open questions for the reader and is a real weakness of the manuscript. With a detection limit of tens of pptv the average abundance of species with absorption in the UV region, like e.g. BTX, formaldehyde, ketones, … can be in the low ppbv range. The selectivity of the current experimental approach is of clear concern here. In the sentence in line 221 this issue is simply discarded and not enough consideration is given to this issue in this manuscript. The implication is that, if the sample air composition is completely unknown, the interference of other species may render this approach inadequate, if it is applied on its own. A balanced discussion of the selectivity aspects, or potential ways to improve it by combination with other techniques, must be included in the manuscript. Finally, in line 220 the campaign data

3

are said to be "quality filtered". If quality filtering means excluding data when formaldehyde mixing ratios were above 5 ppbv, then this is a rather crude way of doing this. Again, there must be a way of also identifying formaldehyde at the same time by other means.

We appreciate the reviewer pointing out that this discussion is not well balanced in the manuscript. The lack of selectivity is a drawback to the UV absorption technique. Given the prevalence of the UV absorption technique in commercial analyzers, much effort has gone into identifying atmospheric species that also absorb in the 265 nm region (see for example the report from 2B Technologies: https://twobtech.com/docs/tech_notes/TN040.pdf). These include aromatic hydrocarbons and other volatile organic compounds (VOC), which can have absorption cross sections approaching that of O_3. Therefore, positive artifacts in O_3 can arise in environments with high VOC, such as within smoke plumes (Long et al., 2020) or in polluted urban environments (Spicer et al., 2010).

We have updated the text in the manuscript to present a more balanced and appropriate discussion of the potential for measurement artifacts:

FIREX-AQ flights targeted forest wildfires and agricultural burns. In fresh, concentrated smoke plumes, UV-active species such as SO_2, aromatic hydrocarbons, and other volatile organic compounds (VOC) can give rise to positive artifacts in the O_3 signal (Long et al., 2020), as the UV absorption technique lacks selectivity (see Birks, 2015). The potential for overestimating O_3 due to interfering absorbers can also be of concern in highly polluted urban environments (e.g., Spicer et al., 2010). In general, these studies demonstrate that UV absorption based O_3 analyzers are not always ideally suited to such applications. Nonetheless, modifications such using an O_3 selective scrubber material (e.g., heated graphite) to preserve VOC and thus account for interferences in the background (I_Z) signal have been shown to reduce positive artifacts (Turnipseed et al., 2017). As we did not substitute the ROZE scrubber for the FIREX-AQ deployment, an on-board, independent measurement of formaldehyde (HCHO) was used as a plume indicator. ROZE O_3 data are therefore quality filtered to remove points sampled within dense smoke plumes using HCHO mixing ratios above 5 ppbv.

12. L230: Cross plot -> Correlation plot

   This has been corrected in the text.

13. L232: Data from 15 extra flights could go into the supplementary material.

   The remaining ROZE and NOyO3 O_3 data from FIREX-AQ are publicly available (https://www-air.larc.nasa.gov/missions/firex-aq/), and the authors feel that providing additional correlation plots does not further the comparison. We have added the range of observed intercepts to the range of observed slopes (text L238).

14. L253: …not shown in Figure 6.

   See response to question 9 above.

15. L257/258: "*Scalar data processing included detrending the scalar mixing ratios by subtracting a 20 second running mean and synchronizing the data with the vertical winds.*" On what basis was that decided. Some more background explanation would be useful here.

The detrend removes any non-turbulent variability in the scalar data. The averaging window was determined empirically by inspection of the co-spectral power (as in Figure 8c) generated from a range of detrending lengths. This data is not shown, but the procedure has been detailed in the text as follows:

L264: *Scalar data were detrended by subtracting a 20 second running mean, which corresponds to spatial scales of ~2.7 km. The detrending length was chosen to remove non-turbulent variability (e.g., changing chemical conditions) while still capturing the largest flux-contributing eddies as identified by examination of the co-spectra from a range of averaging windows. Scalar data were then synchronized to the vertical winds using a time-lag that optimized covariance.*

16. Generally, the manuscript would benefit from a brief and compact comparison with other techniques for ozone detection and how the new ROZE compares in performance with those approaches. This could take the form of a small table. If this turns out to be too formidable, the authors may restrict this comparison to cavity enhanced absorption approaches.

We appreciate the reviewer's desire for context to be provided. The manuscript briefly describes other techniques in the introduction and provides references without detailing their performance characteristics. Our purpose in this manuscript is to demonstrate the capabilities of ROZE, in particular for eddy covariance fluxes, rather than to compare/contrast it to existing technologies. A more detailed comparison is best addressed in a devoted instrument intercomparison or review article, as instrument drawbacks and benefits also depend on the measurement application (cost, weight and size, precision requirements, accuracy requirements, time response, etc) and deserve a more thorough examination.

Technical corrections (small improvements and formal/formatting errors):
The following have been addressed in the text:

Many superscripts (in units) did not come out correctly in print, see lines:
19, 45, 189, 190, 244, 266, 283

L43: Rephrase: … cylinders containing compressed toxic gases and the use of dangerous chemical dyes.

References:
Aubinet et al. – relevant pages might be missing
Birks – typo in titles and reference incomplete
Bourgeois et al. – volume seems to be missing
Ryerson et al. – NO 2 -> NO2 (insert proper index)
Serdyuchenko et al. – ill-defined symbols in my copy
Young et al. – Journal name should not be abbreviated

Table:

Size – unit should read cm3, or X cm x Y cm x Z cm
Precision – typo in value and unit

Figures:
Figure 1
- Even though this figure is only schematic, the way the LED light pulses are drawn is confusing. Pulses arrive at cavity with a 10 Hz repetition rate. At 10 Hz only one pulse is in the cavity at one time. The pulse duration is long enough to draw this figure in CW mode and explain the pulsed nature of ROZE in the text.
- Fig. 1 caption – replace *"long optical pathlength"* by *" long* effective optical pathlength"

Figure 2
Axes titles and colour code could be improved. Axis title for the LED spectrum (normalized intensity) is okay, for the cross-section the chosen (right) axis title is also okay. The figure however also contains the reflectivity spectrum, which is unitless, and thus the title should occur somewhere. The relative intensity axis can of course be used, but the title should be changed to make clear that 3 different quantities are shown. Moreover, the two shades of blue are difficult to distinguish, and do not work in my opinion; modify the color code.

Figure 6
- O3 on the axis title should be indexed properly; i.e. O3.
- In panel (a) it would be better to show an individual pulse and a proper fit rather than 5 pulses, where the fitted data point can hardly be made out. The sentence: "Individual pulses were fit to an exponential decay using the selected data points in red" is not clear. An exponential function is fitted to the experimental data and not vice versa. This should be rephrased.
- What is meant by an "e/3 flush rate"? This is phrased casually.
  See response to question 10 above.

Figure 7
- O3 on both axis titles should be indexed properly; i.e. O3.
- Scatter plot -> Correlation plot
- How does an intercept of "0.17 +/- 0.02 ppbv" agree with the detection limit? Comment.
  See responses to questions 13 and 20.

We would like to thank the Referee for their thoughtful comments. More detailed responses to the comments are outlined below.

COMMENTS TO THE AUTHOR(S): The paper offers a clear and concise description of a new, sensitive, and versatile instrument for the in-situ detection of ozone via UV absorption. The small sample size/rapid flush rate and precision of the instrument enable flux measurements. Comparison/calibration with a reference standard in the laboratory, and comparisons with an established airborne instrument in the field establish its performance characteristics and accuracy. The paper is well written, reasonably comprehensive, and the instrument is a valuable addition to the suite of airborne ozone sensors. Comments, but Mostly Questions:

17. Line 67 (also caption to Fig. 1) - is the light collimated and coupled via high-reflectivity mirrors, or do the high-reflectivity mirrors constitute the optical cavity?

    The high-reflectivity mirrors constitute the optical cavity. The beam is collimated using an aspheric lens. The text and figure caption have been clarified accordingly:

    L67: *As illustrated in Figure 1, a light-emitting diode (LED) in the UV (λ_{max} = 265 nm) is collimated with an aspheric lens and coupled into an optical cavity formed by two high-reflectivity mirrors.*

18. Lines 75+ and 152+ - It is addressed, but I wonder if it is possible to be a bit more explicit here about what is measured (Iz and I?), what is known (Rayleigh and ozone cross sections?) and what has to be empirically determined/calibrated (Leff, which is set by mirror reflectivity?)? Also, how stable is mirror reflectivity over time? Do the Iz measurements at different pressures enable determination of Leff in flight? Are there other atmospheric absorbers in this region? Does the Rayleigh scatter term depend upon the composition of the sample other than ozone, e.g., H2O, CO, CO2? Does the scrubber alter the concentrations of these species?

    The intensity terms (I_z, I) are measured, the Rayleigh and ozone cross sections are known from the literature. The mirror reflectivity dictates the cavity excitinction (a_{cav})/effective pathlength (L_{eff}) and must be empirically determined via calibration. The text has been clarified as follows:

    L85: *In principle, accurate trace gas measurements require calibration of the α_{cav} term yielding L_{eff}, knowledge of the Rayleigh and absorption cross sections in the detected spectral region, and the measured I_0 and I terms.*

    L155: *Using the measured I_Z, I, and the known Rayleigh scatter and O_3 absorption cross sections, the O_3 number density can then be determined as $\alpha_{O3} = N_{O3}\sigma_{O3}$.*

    With adequate particle filtering, the mirror reflectivity is relatively stable over time. Although we do not show the data in the manuscript, calibrations before and after the FIREX-AQ field deployment do not show significant degradation in the optical pathlength. Changes in Iz with pressure during flight could enable real-time calibration.

Other atmospheric absorbers are present in the region. A more detailed discussion of this point can be found in response to question 11 above.

We use the Rayleigh scattering cross section for the standard atmosphere (dry air, 300 ppmv CO_2) as determined by Bucholtz (1995). Given the relatively low ambient mixing ratios of H_2O, CO_2 and CO, the scattering is dominated by interactions with N_2 and O_2. Tomasi et al. (2005) confirm that increasing to ~50% relative humidity and 385 ppmv CO_2 results in a < 0.02% difference in the calculated cross section. Overall, ambient changes in these species contributes only small uncertainty and is lumped into the upper estimate of ± 3% in the Rayleigh cross-section. The Carulite scrubber does not destroy CO_2 or H_2O but does convert CO into CO_2.

19. Lines 105+ - Is the cell surface treated to limit ozone loss? What material is the diffuser (FEP?)? Does the particulate filter lead to ozone loss in the sample? How do you verify the performance of the scrubber? Does its ability to fully scrub ozone depend upon flow rate, ambient pressure, ambient ozone concentrations?

The cell surface is not treated to limit O_3 loss. We have found no evidence of surface O_3 loss during regular operation, and the Rayleigh and O_3 calibrations show good agreement. The diffuser is made of stainless steel which has been added to the text.

We verify the performance of the O_3 scrubber by configuring high O_3 (~ 1 ppmv) and zero O_3 air to flow through it. We find that the resulting detected intensity shows no change with increasing O_3 under both low and high flow conditions.

20. Fig. 7 - Any thoughts on what led to the positive offset between ROZE and NOyO3? At <1% of mixing ratios at 20 ppbv it may not be worth worrying about.

ROZE and NOyO3 did not share a sample line during the FIREX-AQ deployment. Although we cannot conclusively identify the source of the non-zero intercept, NOyO3 sampled from an inlet at the left forebody of the aircraft while ROZE sampled from an inlet on the right, midbody. Perhaps small fluctuations in ambient O_3 could account for some of the observed discrepancy. We have modified the text as follows:

L257: *Note the intercept is less than 1% of the minimum observed O_3 mixing ratios for this flight. Comparisons for 15 flights from the campaign indicate a range of 0.96–1.04 in slope and -1.6–1.4 ppbv O_3 in intercept (in all cases, this offset is < 4% of the minimum measured O_3), consistent with the measurement uncertainty.*

A Cavity-Enhanced UV Absorption Instrument for High Precision, Fast Time Response Ozone Measurements

Reem A. Hannun[1,2], Andrew K. Swanson[1,3], Steven A. Bailey[1], Thomas F. Hanisco[1], T. Paul Bui[4], Ilann Bourgeois[5,6], Jeff Peischl[5,6], Thomas B. Ryerson[5]

[1]Atmospheric Chemistry and Dynamics Laboratory, NASA Goddard Spaceflight Center, Greenbelt, MD, USA
[2]Joint Center for Earth Systems Technology, University of Maryland Baltimore County, Baltimore, MD, USA
[3]Universities Space Research Association, Columbia, MD, USA
[4]Earth Science Division, NASA Ames Research Center, Moffett Field, CA, USA
[5]NOAA Chemical Sciences Laboratory, Boulder, CO, USA
[6]Cooperative Institute for Research in Environmental Sciences, University of Colorado Boulder, Boulder, CO, USA

Correspondence to: Reem A. Hannun (reem.a.hannun@nasa.gov)

Abstract. The NASA Rapid Ozone Experiment (ROZE) is a broadband cavity-enhanced UV absorption instrument for the detection of *in situ* ozone (O_3). ROZE uses an incoherent LED light source coupled to a high-finesse optical cavity to achieve an effective pathlength of ~104 m. Due to its high-sensitivity and small optical cell volume, ROZE demonstrates a 1σ precision of 80 pptv (0.1 s) and 31 pptv (1 s), as well as a $1/e$ response time of 50 ms. ROZE can be operated in a range of field environments, including low- and high-altitude research aircraft, and is particularly suited to O_3 vertical flux measurements using the eddy covariance technique. ROZE was successfully integrated aboard the NASA DC-8 aircraft during July–September 2019 and validated against a well-established chemiluminescence measurement of O_3. A flight within the marine boundary layer also demonstrated flux measurement capabilities, and we observed a mean O_3 deposition velocity of 0.029 ± 0.005 cm s^{-1} to the ocean surface. The performance characteristics detailed below make ROZE a robust, versatile instrument for field measurements of O_3.

1   Introduction

In the troposphere, ozone (O_3) adversely affects air quality and acts as a greenhouse gas. Dry deposition to the Earth's terrestrial and oceanic surfaces represents a significant loss pathway for tropospheric O_3 (Young *et al.*, 2018) and thus influences tropospheric composition and O_3 pollution. Additionally, O_3 uptake through plant stomata leads to vegetation and crop damage (Ainsworth *et al.*, 2012; Mills *et al.*, 2018) and poor ecosystem health (Lombardozzi *et al.*, 2015), potentially amplifying the effects of O_3 on climate (Sitch *et al.*, 2007) and air quality (Sadiq *et al.*, 2017). Despite its role in the tropospheric O_3 budget, dry deposition velocities (v_d) of O_3 remain poorly constrained (Wesely and Hicks, 2000; Hardacre *et al.*, 2015). The observational records of terrestrial $v_d(O_3)$ are limited in number and do not capture the full variability in O_3 deposition rates with land cover (Clifton *et al.*, 2020a). Furthermore, studies of O_3 deposition to the ocean (e.g., Kawa and Pearson, 1989; Faloona *et al.*, 2005; Helmig *et al.*, 2012; Novak *et al.*, 2020) report deposition velocities of ~ 0.01–0.05 cm s^{-1}, which are 1–2 orders of magnitude lower than typical terrestrial values. Observations from Helmig *et al.* (2012) also suggest that O_3 deposition may vary with sea surface temperature. Global chemistry modeling frameworks that incorporate O_3 dry deposition (e.g., Bey *et al.*, 2001; Lamarque *et al.*, 2012) often apply fixed deposition rates to the ocean and heavily parameterized deposition schemes over land (Wesely, 1989). However, process-level representation of O_3 deposition improves agreement between modeled and observed surface O_3 concentrations (Clifton *et al.*, 2020b; Pound *et al.*, 2020). The range and variability in O_3 deposition rates thus motivates the need for further $v_d(O_3)$ measurements to refine both atmospheric and land surface model predictions.

Measurements of vertical O_3 fluxes are typically accomplished via eddy covariance (EC) analysis. The EC technique demands fast time-response, high-precision sensors to resolve the turbulence-driven variability in scalar concentrations. O_3 fluxes are therefore measured using highly sensitive O_3 detection methods such as chemiluminescence (e.g., Bariteau *et al.*, 2010; Muller *et al.*, 2010) and, more recently, chemical ionization mass spectrometry (CIMS) (Novak *et al.*, 2020). Chemiluminescence detectors employ either nitric oxide (NO) gas or organic dyes, which generate photons on reaction with O_3. While these instruments exhibit good sensitivity, they have practical drawbacks involving the use of cylinders containing toxic compressed ~~gas cylinders and~~gases or dangerous chemical dyes. Novak *et al.* (2020) successfully demonstrated the use of oxygen anion CIMS to measure O_3 and its vertical fluxes with a detection limit of < 0.005 cm s^{-1} over the ocean. To the best of our knowledge, ultraviolet (UV) absorption instruments have not previously been utilized for O_3 flux measurements due to insufficient sensitivity (e.g., Gao *et al.*, 2012). However, advancements in incoherent cavity-enhanced absorption spectroscopy (Fiedler *et al.*, 2003) facilitate the development of high-sensitivity sensors that are both robust and compact. Furthermore, UV absorption has the advantage of providing direct detection of O_3 without the need for a chemical titration source.

We report on the development of the NASA Rapid Ozone Experiment (ROZE), a cavity-enhanced UV absorption instrument for the *in-situ* detection of O_3. The long optical pathlength and small cavity volume enable high precision measurements in short averaging times, making ROZE suitable for O_3 flux measurements with the EC technique. The compact instrument design supports integration aboard research aircraft for both tropospheric and stratospheric deployment. We describe the principle of operation along with major instrument components and performance characteristics below. We also discuss the field performance of ROZE and demonstrate its EC capabilities using aircraft observations of O_3 deposition to the ocean surface.

2 Principle of operation

Incoherent broadband cavity-enhanced absorption spectroscopy (IBBCEAS) is an established tool for the detection of trace gas species (Fiedler *et al.*, 2003; Ball *et al.*, 2004; Washenfelder *et al.*, 2008) including O_3 (Darby *et al.*, 2012; Gomez and Rosen, 2013). IBBCEAS relies on a broadband, incoherent light source coupled to a high-finesse optical cavity. Typically, a multi-channel detector resolves structured absorption features in the ultraviolet (UV) or visible spectral regions. IBBCEAS exploits the long optical pathlength generated in the cavity to enhance sensitivity, comparable to other cavity-enhanced methods such as cavity ringdown spectroscopy (CRDS). However, unlike CRDS, IBBCEAS uses a relatively inexpensive light source as compared to a narrow linewidth laser. Furthermore, the incoherent light source relaxes the stringent requirements for cavity alignment that accompany other cavity enhanced methods such as CRDS, enabling a more robust instrument configuration for field environments.

ROZE employs the IBBCEAS technique for high-sensitivity measurements of O_3. As illustrated in Figure 1, a light-emitting diode (LED) in the UV ($\lambda_{max} = 265$ nm) is collimated with an aspheric lens and coupled into an optical cavity ~~via~~formed by two high-reflectivity mirrors. Exiting light is passed to a photomultiplier tube (PMT) detector through a series of collection and filter optics. Figure 2 depicts the normalized detected LED intensity, which accounts for the LED spectral irradiance, the optical bandpass filter transmission, and the wavelength dependent PMT response. The LED spectrum overlaps with the O_3 Hartley band, and any O_3 present in the sample cell attenuates the light intensity received at the detector. The use of optical filters on the PMT precludes the need for wavelength resolution from a grating spectrometer and simplifies data reduction. Section 3.1 provides further details on the ROZE optical system.

2

Attenuation of light intensity in an IBBCEAS cavity results from trace gas absorption as well as extinction due to the mirrors and Rayleigh scatter. Accounting for these additional losses, the Beer-Lambert absorption coefficient, α_{abs}, is related to the observed change in intensity transmitted through the cavity as follows (Washenfelder *et al.*, 2008):

$$\alpha_{abs} = \left(\frac{I_0 - I}{I}\right)\left(\frac{1-R}{d} + \alpha_{Ray}\right) \tag{1}$$

Here, I_0 is light intensity in the absence of any absorbing species, I is the intensity attenuated due to absorption, R is the mirror reflectivity, d is the physical distance separating the cavity mirrors, and α_{Ray} is the extinction due to Rayleigh scatter, a non-negligible component in the UV. The term $(1 - R)/d$ gives the theoretical cavity loss, α_{cav}, and represents the inverse of the maximum effective pathlength, L_{eff}. In cavity-enhanced techniques, L_{eff} can be many orders of magnitude larger than d, resulting in high sensitivity to the absorbing species. Equation 1 can also be expressed as $\alpha_{abs} = N\sigma_{abs}$, where N is number density of the absorbing species and σ_{abs} is the absorption cross section. In principle, accurate trace gas measurements require calibration of the α_{cav} term~~, as well as~~ yielding L_{eff}. knowledge of the Rayleigh and absorption cross sections in the detected spectral region, and the measured I_0 and I terms. The data processing and calibration for ROZE will be discussed in Sections 3.4 and 4.1, respectively.

3 Instrument description

ROZE consists of three main subsystems housed in a compact 58 cm long x 44 cm wide x 18 cm high chassis, with a total instrument weight of 19 kg (Figure 3). The optical plate – a custom aluminum honeycomb panel supported by friction dampened spring vibration isolators – provides a stable platform for the optical components, consisting of the LED, sample cell, and PMT. The remaining subsystems include the flow handling and the data acquisition. Each major subsystem is described in greater detail below. ROZE operates at 24 V_{DC} with a low-profile AC-DC switching power supply (Vicor VI-LU3-IU) capable of running off 115 or 230 V_{AC} (47–440 Hz), which can be supplied directly from the aircraft. Power consumption is less than 200 W and typically ~100 W. Table 1 summarizes ROZE design and performance characteristics.

3.1 Optical components

3.1.1 LED assembly

A UV LED (λ_{max} = 265 nm, FWHM = 10 nm) (Thorlabs M265D2) is mounted to a custom heat sink and temperature controlled to 30 °C with a thermo-electric cooler (TE Technology CH-21-1.0-1.3; Wavelength Electronics PTC2.5K-CH). The LED output power is separately monitored by a photodiode (Marktech MTPD4400D-1.5) inserted into the edge of a lens tube that holds the LED. The LED assembly attaches to a custom cage mount system that also houses the associated optics, including the aspheric collimation lens (f = 79 mm, Thorlabs ASL10142M) and a beam expander (Thorlabs BE02-UVB) in reverse to shrink the collimated LED output. For compactness, the LED assembly and cage system are mounted parallel to the sample cell, and two mirrors (Thorlabs NB1-K04) ~~direct~~turn the beam 180° into the cell (see Figure 3).

3.1.2 Sample cell

The sample cell is manufactured from an aluminum alloy tube measuring 30 cm in length with a 1.2 cm inner diameter. The cell mirrors (Layertech 109561) have a reflectivity of R > 99.7% over the detected spectral range (Figure 2) and a 500 mm radius of curvature. The mirrors are held directly at the cell ends on face type o-ring seals using custom, non-adjustable mounts fastened to tube collars. The mirror positions are configured to maximize centricity. Two gas ports direct the sample flow into and out of the cell at right angles. The sample enters through a custom stainless steel cylindrical diffuser, a ring with circumferential openings

adjacent to the cell mirrors, that nests within the cell tube orthogonal to the ports. The diffuser helps minimize noise due to Rayleigh scatter from turbulence within the cell at high sample flow rates. A 2-micron pleated mesh filter (Swagelock) affixes to the sample cell inlet port to exclude dust and other particles from affecting the mirror reflectivity, as the mirrors are not independently purged. A pressure transducer (Omega MMA015V10P4K1T4A6) measures the cell pressure from a port near the cell center. The entire cell is thermally regulated to 35 °C using resistive heaters and a precision heater control (Wavelength Electronic PTC2.5K-CH).

3.1.3 PMT assembly

A PMT (Hamamatsu H10720-113) operating in analog mode collects the light exiting the cell. Two optical bandpass filters (Thorlabs FGUV5-UV, Semrock FF01-260/16) transmit the cell output to a collection lens (f = 35 mm, Thorlabs LA4052-UV), which images the beam onto the PMT photocathode. A UV window (Thorlabs WG40530-UV) glued into a custom PEEK lens tube adapter seals to the PMT face with a Viton gasket, creating a leak-tight package for low-pressure (high-altitude) operation. The PMT is thermally stabilized to 35 °C in the same manner as the sample cell. The PMT signal is passed to an amplifier circuit (Analog Devices EVAL-ADA4625-1ARDZ) before digitization by the data acquisition system described below.

3.2 Flow system

The ROZE flow system is designed to achieve rapid flushing of the detection cell as required for fast concentration measurements. However, ROZE samples at ambient pressure to maximize sensitivity, necessitating high throughput with a minimal pressure differential. ROZE utilizes a linear diaphragm pump (Thomas 6025SE-150113) that can achieve a flow rate of up to 18 standard liters per minute (SLM) through the system. The pump speed can also be adjusted by varying the supply current and has three pre-set speeds (e.g., 2, 5, 11 SLM) that can be changed by a switch on the chassis front panel. A flow meter (Honeywell AWM5104) located between the cell exhaust and the pump monitors the sample flow in real time. ROZE uses fluorinated ethylene propylene (FEP) tubing both external and internal to the chassis upstream of the sample cell. External to the chassis, the inlet details depend on the aircraft platform. ROZE has previously used the inlet detailed in Cazorla *et al.* (2015) when flying on the NASA DC-8 aircraft. The instrument exhaust plumbs directly to an exhaust port near the rear of the aircraft. To exclude dust and other particles from affecting the mirror reflectivity, a 2 micron pleated mesh filter (Swagelock) affixes to the sample cell inlet port. More aggressive filtering can be achieved at the cost of reduced (< 18 SLM) flow rates but may be necessary depending on the environment and if O_3 deposition measurements are not the primary goal.

ROZE O_3 measurements also require knowledge of the reference intensity (I_0) as detailed in Equation 1. A 3-way solenoid valve (NResearch TC648T032) switches between the sample line (ambient air from the aircraft inlet) and the zero port, which attaches to an internal Carulite O_3 scrubber (2B Technologies) to produce O_3-free air. Periodic zeroing during operation captures long-term drift in I_0 due to the LED output, PMT response, and changing environmental conditions. Typically, the instrument opens to the O_3 scrubber for 10 seconds every 5 minutes.

3.3 Data acquisition

ROZE utilizes a CompactRIO (National Instruments cRIO-9030) that incorporates a real-time operating system and a Field Programmable Gate Array (FPGA). The FPGA is configured for modulation of the LED and subsequent digitization of the PMT signal. To improve measurement precision and remove background due to ambient light scatter, the FPGA modulates the LED at 1 kHz with a 90% duty cycle (900 μs ON/100 μs OFF) via an external LED driver (Wavelength Electronics FL591FL). A 16-bit Analog to Digital Converter (ADC) digitizes the amplified PMT signal at a digitization rate of 100 kHz. This high rate enables us

4

to average each LED ON and OFF pulse amplitude. We then take the difference of the ON and OFF signals to remove background noise, both optical (i.e., stray light) and electronic. The 1 kHz differences are further averaged to 10 Hz and recorded. Other diagnostic housekeeping variables (e.g., sample flow, temperatures, LED power) are recorded at 1 Hz. Additionally, an analog output commands the 3-way valve to open to the zero line with a user-defined period and duration.

3.4 Data processing

In practice, the absorbance calculation for ROZE factors in the pressure difference between the sample and zero lines, as derived by Min *et al.* (2016):

$$\alpha_{O3} = \left(\frac{I_Z}{I} - 1\right)\left(\alpha_{cav} + \alpha_{Ray,Z}\right) + \Delta\alpha_{Ray} \tag{2}$$

Analogous to Equation 1, I_Z is the intensity measured when sampling through the zero line (O$_3$-scrubbed air), I is the intensity when sampling ambient air, and $\Delta\alpha_{Ray} = \alpha_{Ray,Z} - \alpha_{Ray,S}$, where $\alpha_{Ray,Z}$ and $\alpha_{Ray,S}$ give the Rayleigh extinction ($\alpha_{Ray} = N_{air}\sigma_{Ray}$) of the zero and the sample respectively. Using the measured I_Z, I, and the known Rayleigh scatter and O$_3$ absorption cross sections, the O$_3$ number density can then be determined as $\alpha_{O3} = N_{O3}\sigma_{O3}$. The Rayleigh scattering (Bucholtz, 1995) and O$_3$ absorption (Serdyuchenko *et al.*, 2014) cross sections are calculated as the weighted average over the collected spectral range (Figure 2). Using known cross sections and a calibrated α_{cav} (inverse effective pathlength), the observed change in intensity yields a direct measure of the O$_3$ concentration.

4 Performance

4.1 Sensitivity and calibration

The effective pathlength of the ROZE optical cavity determines the instrument sensitivity to O$_3$ (i.e., the attenuation in intensity per unit O$_3$). The cavity extinction, and thus the effective pathlength, are dictated by the mirror reflectivity as described above but require independent calibration. Calibration can be accomplished via standard addition of O$_3$ or Rayleigh attenuation (in the absence of absorbing species) at varied sample pressures. The former method relies on commercially available O$_3$ generators or sensors for verification, which lack the required accuracy and may drift over time. In contrast, the Rayleigh calibration provides a convenient and straightforward alternative. Both methods are described below.

Figure 4a depicts the ROZE calibration using known concentrations of O$_3$. A commercial O$_3$ source (2B Technologies 306) generated known amounts of O$_3$, with the zero O$_3$ addition serving as the I_Z baseline. Per Equation 2, the slope of the observed attenuation ($dI = I_Z/I - 1$) as a function of O$_3$ number density is proportional to the remaining extinction terms ($\alpha_{cav} + \alpha_{Ray}$). Solving for α_{cav} using the O$_3$ cross section and the calculated Rayleigh extinction, the calibration yields an effective pathlength of $L_{eff} = 108 \pm 6$ m. The alternate calibration uses the Rayleigh extinction in zero air over a range of cell pressures (Figure 4b). In the absence of absorbing species, an expression for α_{cav} can be derived following the approach in Washenfelder *et al.* (2008) as:

$$\alpha_{Ray} = \left(\frac{I_0}{I} - 1\right)\alpha_{cav} \tag{3}$$

I_0 represents the intensity at vacuum, which can be extrapolated from a linear fit of counts as a function of cell pressure. The slope of the observed change in intensity with number density therefore yields a direct measure of the cavity extinction, resulting in an effective pathlength of 104 ± 4 m. The two methods agree to within fit uncertainties, and we use L_{eff} as determined by the Rayleigh calibration for subsequent calculations.

5

4.2   Precision and accuracy

The major contributions to instrument noise include PMT electrical noise and differential scatter or absorption due to non-uniform flow within the sample cell at high flow rates. The flow diffuser (see Section 3.1.2) effectively reduces the flow noise, while decreasing the gain on the PMT amplifier circuit minimizes the PMT electrical noise. The ROZE precision can be determined from the continuous sampling of zero air at a constant pressure. Figure 5 depicts a 1σ Allan deviation plot for ROZE (in pptv O_3 equivalents) as calculated from optical extinction measurements of zero air acquired over 1.5 hours at 944 mbar. For short integration times (< 10 s), a fit of the data gives a $\tau^{-0.47}$ decay, indicating the Allan deviation closely follows the square root of the averaging time ($\tau^{-1/2}$) as expected for white noise. At the native 0.1 s sampling rate, the 1σ precision for O_3 is 80 pptv and reduces to 31 pptv with 1 s averaging. For the given cell pressure and a temperature of 35 °C, this translates to a 1σ precision of 6.7 x 10^8 molecules cm^{-3} (1 s average) of O_3.

The absolute accuracy of the ROZE measurement depends on uncertainties in the literature-reported values of the O_3 and Rayleigh cross sections, the measured cell temperature and pressure, and the calibrated cavity extinction. The reported O_3 absorption cross section has an uncertainty of 2% (Gorshelev *et al.*, 2014), and we estimate an upper uncertainty of 3% for the Rayleigh scattering cross section (Bucholtz, 1995). The cell pressure and temperature are accurate to within 0.2% and 0.5% respectively, and the calibrated cavity extinction has an additional 4% slope uncertainty from the linear fit. These errors propagate through Equation 2 to yield a total measurement uncertainty of 6.2% in the O_3 number density.

4.3   Response time

The flush time of the sample cell limits the true instrument response time despite the 10 Hz data acquisition rate. A rapid flush rate is critical for high spatial resolution measurements from a fast-moving platform. Additionally, fast concentration measurements are required for sampling of turbulent eddies for airborne EC, and the necessary time response scales with aircraft speed. Response times of 10 Hz are typically considered sufficient for ground-based EC (Aubinet *et al.*, 2012), while for airborne EC, a response times of 1–5 Hz are typically sufficient due to larger eddy scales at altitude (Wolfe *et al.*, 2018). Figure 6a shows the instantaneous instrument response to a series of 10 ms pulses of O_3 injected into a zero-air carrier flow using a fast switching valve (The Lee Company, IEP series). During this experiment, the pump maintained a sample flow rate of 18 SLM. A series of exponential decay fits for several O_3 pulses yields an *e*-folding time constant of $\tau_r = 50 \pm 4$ ms (Figure 6b). The time ~~constant~~to flush the cell to $1/3e$ of its initial contents thus corresponds to a ~~3*e*-fold~~ flush rate of 9.5 Hz.

5   Field demonstration

ROZE can be operated on both low- and high-altitude aircraft platforms. Though ROZE has not yet flown on a high-altitude unpressurized aircraft (such as the NASA ER-2), laboratory experiments in a thermal vacuum chamber have demonstrated no loss of performance down to a pressure and temperature of 50 mbar and 250 K (results not shown). In summer 2019, ROZE flew aboard the NASA DC-8 for the Fire Influence on Regional to Global Environments Experiment, Air Quality (FIREX-AQ) campaign over the Central and Northwest United States. ~~Campaign flights targeted smoke plumes from forest wildfires and agricultural burns.~~ The instrument operated as described above, with the addition of an inline particle filter (Balston 9922-05-DQ) to protect the cavity mirrors from fine particulates in the ~~smoke. In fresh, concentrated smoke plumes, UV active species such as SO₂ and aromatic hydrocarbons can give rise to positive artifacts in the O₃ absorption measurement (Birks, 2015). This is a drawback to the UV absorption measurement, which can be affected by both absorbing and scattering molecules. However, such UV active absorbers~~

220 ~~are generally not abundant enough in the background atmosphere to be of concern. The FIREX-AQ ROZE data are therefore quality filtered to remove points sampled within dense smoke plumes using observed formaldehyde mixing ratios above 5 ppbv.~~ targeted smoke plumes. Although more aggressive filtering comes at the cost of reduced flow rates and thus lowers the instrument response time, O_3 deposition measurements were not a primary objective of FIREX-AQ. Below, we detail comparisons of ROZE against an established O_3 measurement. Additionally, level flight legs in the marine boundary layer during a flight over

225 the ocean provide an initial demonstration of O_3 vertical flux measurements.

5.1 **FIREX-AQ** validation against chemiluminescence

FIREX-AQ flights targeted forest wildfires and agricultural burns. In fresh, concentrated smoke plumes, UV-active species such as SO_2, aromatic hydrocarbons, and other volatile organic compounds (VOC) can give rise to positive artifacts in the O_3 signal (Long *et al.*, 2020), as the UV absorption technique lacks selectivity (see Birks, 2015). The potential for overestimating O_3 due to

230 interfering absorbers can also be of concern in highly polluted urban environments (e.g., Spicer *et al.*, 2010). In general, these studies demonstrate that UV absorption based O_3 analyzers are not always ideally suited to such applications. Nonetheless, modifications such using an O_3 selective scrubber material (e.g., heated graphite) to preserve VOC and thus account for interferences in the background (I_z) signal have been shown to reduce positive artifacts (Turnipseed *et al.*, 2017). As we did not substitute the ROZE scrubber for the FIREX-AQ deployment, an on-board, independent measurement of formaldehyde (HCHO)

235 was used as a plume indicator. ROZE O_3 data are therefore quality filtered to remove points sampled within dense smoke plumes using HCHO mixing ratios above 5 ppbv.

The DC-8 FIREX-AQ payload included the NOAA Nitrogen Oxides and Ozone (NOyO3) instrument, a well-established O_3 measurement using the chemiluminescence technique (Ryerson *et al.*, 2000; Bourgeois *et al.*, 2020). ROZE operated

240 simultaneously with the NOyO3 instrument during several flights. Figure 7 shows a comparison of ROZE and NOyO3 data for the July 30, 2019 flight over the Northwestern United States. During this flight, no fresh smoke plumes were sampled, and no filtering of the ROZE data was necessary. Figure 7a depicts a ~25 min subset of the full timeseries to illustrate the ROZE instrument precision. Both measurements (averaged to 1 s) track the dynamic features in O_3 mixing ratios well. The ~~cross~~ correlation plot for the full flight (Figure 7b) demonstrates strong agreement between the two measurements, with a slope of 0.98 ± 0.01 and an

245 intercept of 0.17 ± 0.02 ppbv O_3 (r^2 = 0.99). Note the intercept is less than 1% of the minimum observed O_3 mixing ratios for this flight. Comparisons for 15 flights from the campaign indicate a range of 0.96–1.04 in slope and -1.6–1.4 ppbv O_3 in intercept (in all cases, this offset is < 4% of the minimum measured O_3), consistent with the measurement uncertainty.

5.2 Ozone flux measurements

5.2.1 Eddy covariance flux

250 The vertical flux of O_3 can be directly quantified using the eddy covariance (EC) technique. EC defines the flux (F) as the time or spatially averaged covariances in the vertical wind speed (w) and the scalar species of interest (in this case the O_3 mixing ratio X_{O3}):

$$F_{O3} = \langle w'X_{O3}' \rangle \tag{4}$$

In the equation above, the primes denote instantaneous deviations from the mean value, and the brackets indicate an average over

255 a prescribed interval as discussed below. Since deposition dominates transfer across the air-surface interface, the O_3 flux can instead be expressed as a transfer rate or deposition velocity (v_d):

7

$$v_d = -\frac{F_{O3}}{\bar{X}_{O3}} \hspace{7cm} (5)$$

Here, the overbar indicates the mean O_3 mixing ratio over the averaging period. The deposition velocity, in units of cm s^{-1}, yields a normalized metric of the deposition efficiency and incorporates both chemical and physical transfer processes.

During the FIREX-AQ campaign, the flight on July 17, 2019 contained a level segment within the turbulent marine boundary layer suitable for EC. The flux transects were located over the Pacific Ocean, ~200 miles southwest of the Los Angeles Basin. To quantify O_3 deposition, the Meteorological Measurement System (MMS) instrument provided 3-D wind vector data (Chan *et al.*, 1998), which were used in conjunction with ROZE O_3 measurements. A 1-D coordinate rotation was applied to the wind vector to force the mean vertical wind to zero, and the native 20 Hz MMS data was averaged to the ROZE 10 Hz time base. Note that the additional particle filter reduced the ROZE sample flow to 11.3 SLM, and we estimate the time constant from the decay ~~of~~in intensity following the zero-O_3 additions as τ_r = 90 ms (5.5 Hz ~~1/3e~~ flush rate~~)~~. (1/3e)). We also use 20 Hz water vapor measurements from the open path Diode Laser Hygrometer (DLH) (Diskin *et al.*, 2002) as a benchmark for the flux performance. 20 Hz DLH data were averaged to the ROZE time base and used to apply a moist-to-dry air correction for raw O_3 observations, negating the need for density corrections to the calculated flux (Webb *et al.*, 1980). This density correction reduces the O_3 flux by ~6%. For the EC calculations, we selected two ~50 km transects with consistent aircraft heading, stationary flow, and level altitude (~170 m). Scalar data ~~processing included detrending the scalar mixing ratios~~were detrended by subtracting a 20 second running mean ~~and synchronizing~~, which corresponds to spatial scales of ~2.7 km. The detrending length was chosen to remove non-turbulent variability (e.g., changing chemical conditions) while still capturing the largest flux-contributing eddies as identified by examination of the co-spectra from a range of averaging windows. Scalar data ~~with~~were then synchronized to the vertical winds~~.~~ using a time-lag that optimized covariance.

5.2.2 Spectral analysis

Spectral analysis aids in decomposing the contributions of eddies at different scales (frequencies) to the overall signal and provides a quality assessment of the ROZE flux measurements. Figure 8 displays the lag-covariance, power spectrum, and co-spectrum for O_3 and vertical wind fluctuations generated using fast Fourier transforms (FFTs) for a single transect. The spectra for water vapor are also displayed for comparison. The lagged cross-cross covariance functions (Figure 8a) demonstrate defined peaks at lags of < 0.5 s, with the peak non-normalized covariance yielding a measure of the flux. Dividing out the background O_3 mixing ratio of 29 ppbv, we find a mean deposition velocity of 0.029 cm s^{-1} for the two transects. The power spectra in Figure 8b show that vertical winds follow the theoretical $f^{-5/3}$ decay expected in the inertial subrange (Kaimal *et al.*, 1972). The slope for the O_3 power spectrum initially follows the same decay but flattens at ~1 Hz, indicating that the turbulence-driven variability in O_3 approaches the ROZE precision limit in higher-frequency eddies. However, the normalized frequency-weighted co-spectral power of w' with X_{O3}' (Figure 8c, solid lines) show that flux carrying eddies below ~0.6 Hz dominate the total signal. The ogive, the cumulative integral of the co-spectrum (Fig. 8c, dashed lines) further indicates that 99% of flux carrying eddies occur at frequencies below ~4 Hz. These results demonstrate the adequate ROZE time response for airborne EC.

5.2.3 Flux measurement uncertainty

Detailed methods to quantify flux errors for airborne EC can be found elsewhere (Lenschow *et al.*, 1994; Langford *et al.*, 2015; Wolfe *et al.*, 2018). Here, we aim to quantify the random and systematic flux errors that reflect the overall instrument performance. We use the empirical formulation of Finkelstein and Sims (2001) to estimate the total random error (RE$_{TOT}$) as the variance of the

scalar-wind covariance. In this approach, the RE_{TOT} is determined using auto- and cross-correlation functions (as in Figure 8a) over lag times that are sufficient to capture the timescale of the correlation (here ~10 s). Averaging over the flux legs yields a RE_{TOT} of 0.005 cm s^{-1}. RE_{TOT} encompasses both instrument noise as well as error from the random sampling of turbulence. To isolate the RE component due solely to instrument noise (RE_{noise}), we follow the approach of Mauder *et al.* (2013). In this method, the standard deviation of the instrument noise is derived from the scalar auto-covariance and then propagated to determine its contribution to the to the cross-covariance uncertainty. Note that RE_{noise} still depends on the turbulence regime and therefore varies with atmospheric conditions. We calculate RE_{noise} to be 0.0015 cm s^{-1} averaging over the two flux transects. These results indicate that instrument noise constitutes ~30% of the total random error.

Additionally, the instrument time response can lead to systematic flux errors as a consequence of under sampling contributions from high-frequency eddies. We determine the systematic error due to the instrument response time (SE_{RT}) following the Horst (1997) model, whereby the attenuation in the measured signal can be expressed as a co-spectral transfer function based on the characteristic instrument response time. Using the ROZE response time of τ_r = 90 ms, we determine SE_{RT} as < 2%, indicating minimal attenuation in the measured flux signal.

6   Summary and conclusions

The NASA ROZE instrument provides high sensitivity, fast time response measurements of O_3 via broadband cavity-enhanced UV absorption. The compact, robust instrument package is adaptable to diverse field environments, including low- and high-altitude aircraft platforms. ROZE currently achieves a 1σ precision of ~30 pptv s^{-1} and an overall accuracy of 6.2%. ROZE was successfully integrated aboard the NASA DC-8 aircraft, and the field performance compares favorably with an independent O_3 measurement to within ROZE uncertainty. The maximum observed time response for laboratory tests was 50 ms, with additional filtering during aircraft operation slowing the time response to 90 ms. The instrument precision and time response make ROZE particularly well suited for vertical O_3 flux measurements using eddy covariance analysis. ROZE has measured O_3 deposition velocities of 0.029 ± 0.005 cm s^{-1} to the ocean surface, with minimal (< 2%) response-time attenuation in the flux signal. The demonstrated performance of ROZE makes the instrument an ideal and versatile option for field measurements of both O_3 concentrations and fluxes.

Data availability

Acknowledgements

References

330   Ainsworth, E. A. *et al.* (2012) 'The Effects of Tropospheric Ozone on Net Primary Productivity and Implications for Climate Change', *Annual Review of Plant Biology*, 63(1), pp. 637–661. doi: 10.1146/annurev-arplant-042110-103829.

Aubinet, M., Vesala, T. and Papale, D. (eds) (2012) *Eddy Covariance*, *Eddy Covariance: A Practical Guide to Measurement and Data Analysis*. Dordrecht: Springer Netherlands. doi: 10.1007/978-94-007-2351-1.

Ball, S. M., Langridge, J. M. and Jones, R. L. (2004) 'Broadband cavity enhanced absorption spectroscopy using light emitting
335   diodes', *Chemical Physics Letters*, 398(1–3), pp. 68–74. doi: 10.1016/j.cplett.2004.08.144.

Bariteau, L. *et al.* (2010) 'Determination of oceanic ozone deposition by ship-borne eddy covariance flux measurements', *Atmospheric Measurement Techniques*, 3(2), pp. 441–455. doi: 10.5194/amt-3-441-2010.

Bey, I. *et al.* (2001) 'Global modeling of tropospheric chemistry with assimilated meteorology: Model description and evaluation', *Journal of Geophysical Research: Atmospheres*, 106(D19), pp. 23073–23095. doi: 10.1029/2001JD000807.

340   Birks, J. (2015) *UV-Abosorbing Interferences in Ozone Monitors*. Available at: https://twobtech.com/docs/tech_notes/TN040.pdf.

Bourgeois, I. *et al.* (2020) 'Global-scale distribution of ozone in the remote troposphere from the ATom and HIPPO airborne field missions', *Atmospheric Chemistry and Physics*, 20(17), pp. 10611–10635. doi: 10.5194/acp-20-10611-2020.

Bucholtz, A. (1995) 'Rayleigh-scattering calculations for the terrestrial atmosphere', *Applied Optics*, 34(15), p. 2765. doi: 10.1364/AO.34.002765.

345   Cazorla, M. *et al.* (2015) 'A new airborne laser-induced fluorescence instrument for in situ detection of formaldehyde throughout the troposphere and lower stratosphere', *Atmospheric Measurement Techniques*, 8(2), pp. 541–552. doi: 10.5194/amt-8-541-2015.

Chan, K. R. *et al.* (1998) 'Turbulence measurements by the DC-8 Meteorological Measurement System', *Geophysical Research Letters*, 25(9), pp. 1355–1358. doi: 10.1029/97GL03590.

Clifton, Olivia E. *et al.* (2020) 'Dry Deposition of Ozone Over Land: Processes, Measurement, and Modeling', *Reviews of*
350   *Geophysics*, 58(1). doi: 10.1029/2019RG000670.

Clifton, O. E. *et al.* (2020) 'Influence of Dynamic Ozone Dry Deposition on Ozone Pollution', *Journal of Geophysical Research: Atmospheres*, p. e2020JD032398. doi: 10.1029/2020jd032398.

Darby, S. B., Smith, P. D. and Venables, D. S. (2012) 'Cavity-enhanced absorption using an atomic line source: application to deep-UV measurements', *The Analyst*, 137(10), p. 2318. doi: 10.1039/c2an35149h.

355   Diskin, G. S. *et al.* (2002) 'Open-path airborne tunable diode laser hygrometer', in Fried, A. (ed.) *Proc SPIE, Diode Lasers and Applications in Atmospheric Sensing*, p. 196. doi: 10.1117/12.453736.

Faloona, I. *et al.* (2005) 'Observations of Entrainment in Eastern Pacific Marine Stratocumulus Using Three Conserved Scalars', *Journal of the Atmospheric Sciences*, 62(9), pp. 3268–3285. doi: 10.1175/JAS3541.1.

Fiedler, S. E., Hese, A. and Ruth, A. A. (2003) 'Incoherent broad-band cavity-enhanced absorption spectroscopy', *Chemical*
360   *Physics Letters*, 371(3–4), pp. 284–294. doi: 10.1016/S0009-2614(03)00263-X.

Finkelstein, P. L. and Sims, P. F. (2001) 'Sampling error in eddy correlation flux measurements', *Journal of Geophysical Research: Atmospheres*, 106(D4), pp. 3503–3509. doi: 10.1029/2000JD900731.

Gao, R. S. *et al.* (2012) 'A compact, fast UV photometer for measurement of ozone from research aircraft', *Atmospheric Measurement Techniques*, 5(9), pp. 2201–2210. doi: 10.5194/amt-5-2201-2012.

365   Gomez, A. L. and Rosen, E. P. (2013) 'Fast response cavity enhanced ozone monitor', *Atmospheric Measurement Techniques*, 6(2), pp. 487–494. doi: 10.5194/amt-6-487-2013.

Gorshelev, V. *et al.* (2014) 'High spectral resolution ozone absorption cross-sections – Part 1: Measurements, data analysis and comparison with previous measurements around 293 K', *Atmospheric Measurement Techniques*, 7(2), pp. 609–624. doi: 10.5194/amt-7-609-2014.

370   Hardacre, C., Wild, O. and Emberson, L. (2015) 'An evaluation of ozone dry deposition in global scale chemistry climate models', *Atmospheric Chemistry and Physics*, 15(11), pp. 6419–6436. doi: 10.5194/acp-15-6419-2015.

Helmig, D. *et al.* (2012) 'Atmosphere-ocean ozone fluxes during the TexAQS 2006, STRATUS 2006, GOMECC 2007, GasEx 2008, and AMMA 2008 cruises', *Journal of Geophysical Research: Atmospheres*, 117(D4). doi: 10.1029/2011JD015955.

Horst, T. W. (1997) 'A simple formula for the attenuation of eddy fluxes measured with first-order-response scalar sensors',
375   *Boundary-Layer Meteorology*, 82(2), pp. 219–233. doi: 10.1023/A:1000229130034.

Kaimal, J. C. *et al.* (1972) 'Spectral characteristics of surface-layer turbulence', *Quarterly Journal of the Royal Meteorological Society*, 98(417), pp. 563–589. doi: 10.1002/qj.49709841707.

Kawa, S. R. and Pearson, R. (1989) 'Ozone budgets from the dynamics and chemistry of marine stratocumulus experiment', *Journal of Geophysical Research*, 94(D7), p. 9809. doi: 10.1029/JD094iD07p09809.

Lamarque, J.-F. *et al.* (2012) 'CAM-chem: description and evaluation of interactive atmospheric chemistry in the Community Earth System Model', *Geoscientific Model Development*, 5(2), pp. 369–411. doi: 10.5194/gmd-5-369-2012.

Langford, B. *et al.* (2015) 'Eddy-covariance data with low signal-to-noise ratio: time-lag determination, uncertainties and limit of detection', *Atmospheric Measurement Techniques*, 8(10), pp. 4197–4213. doi: 10.5194/amt-8-4197-2015.

Lenschow, D. H., Mann, J. and Kristensen, L. (1994) 'How Long Is Long Enough When Measuring Fluxes and Other Turbulence Statistics?', *Journal of Atmospheric and Oceanic Technology*, 11(3), pp. 661–673. doi: 10.1175/1520-0426(1994)011<0661:HLILEW>2.0.CO;2.

Lombardozzi, D. *et al.* (2015) 'The influence of chronic ozone exposure on global carbon and water cycles', *Journal of Climate*, 28(1), pp. 292–305. doi: 10.1175/JCLI-D-14-00223.1.

Long, R. W. *et al.* (2020) 'Comparison of Ozone Measurement Methods in Biomass Burning Smoke: An evaluation under field and laboratory conditions', *Atmospheric Measurement Techniques Discussions*, 2020, pp. 1–33. doi: 10.5194/amt-2020-383.

Mauder, M. *et al.* (2013) 'A strategy for quality and uncertainty assessment of long-term eddy-covariance measurements', *Agricultural and Forest Meteorology*, 169, pp. 122–135. doi: 10.1016/j.agrformet.2012.09.006.

Mills, G. *et al.* (2018) 'Ozone pollution will compromise efforts to increase global wheat production', *Global Change Biology*, 24(8), pp. 3560–3574. doi: 10.1111/gcb.14157.

Min, K.-E. *et al.* (2016) 'A broadband cavity enhanced absorption spectrometer for aircraft measurements of glyoxal, methylglyoxal, nitrous acid, nitrogen dioxide, and water vapor', *Atmospheric Measurement Techniques*, 9(2), pp. 423–440. doi: 10.5194/amt-9-423-2016.

Muller, J. B. A. *et al.* (2010) 'Sources of uncertainty in eddy covariance ozone flux measurements made by dry chemiluminescence fast response analysers', *Atmospheric Measurement Techniques*, 3(1), pp. 163–176. doi: 10.5194/amt-3-163-2010.

Novak, G. A., Vermeuel, M. P. and Bertram, T. H. (2020) 'Simultaneous detection of ozone and nitrogen dioxide by oxygen anion chemical ionization mass spectrometry: a fast-time-response sensor suitable for eddy covariance measurements', *Atmospheric Measurement Techniques*, 13(4), pp. 1887–1907. doi: 10.5194/amt-13-1887-2020.

Pound, R. J. *et al.* (2020) 'Influences of oceanic ozone deposition on tropospheric photochemistry', *Atmospheric Chemistry and Physics*, 20(7), pp. 4227–4239. doi: 10.5194/acp-20-4227-2020.

Ryerson, T. B., Williams, E. J. and Fehsenfeld, F. C. (2000) 'An efficient photolysis system for fast-response NO2 measurements', *Journal of Geophysical Research: Atmospheres*, 105(D21), pp. 26447–26461. doi: 10.1029/2000JD900389.

Sadiq, M. *et al.* (2017) 'Effects of ozone–vegetation coupling on surface ozone air quality via biogeochemical and meteorological feedbacks', *Atmospheric Chemistry and Physics*, 17(4), pp. 3055–3066. doi: 10.5194/acp-17-3055-2017.

Serdyuchenko, A. *et al.* (2014) 'High spectral resolution ozone absorption cross-sections – Part 2: Temperature dependence', *Atmospheric Measurement Techniques*, 7(2), pp. 625–636. doi: 10.5194/amt-7-625-2014.

Sitch, S. *et al.* (2007) 'Indirect radiative forcing of climate change through ozone effects on the land-carbon sink', *Nature*, 448(7155), pp. 791–794. doi: 10.1038/nature06059.

Spicer, C. W., Joseph, D. W. and Ollison, W. M. (2010) 'A Re-Examination of Ambient Air Ozone Monitor Interferences', *Journal of the Air & Waste Management Association*, 60(11), pp. 1353–1364. doi: 10.3155/1047-3289.60.11.1353.

Turnipseed, A. A. *et al.* (2017) 'Use of a heated graphite scrubber as a means of reducing interferences in UV-absorbance measurements of atmospheric ozone', *Atmospheric Measurement Techniques*, 10(6), pp. 2253–2269. doi: 10.5194/amt-10-2253-2017.

Washenfelder, R. A. *et al.* (2008) 'Measurement of glyoxal using an incoherent broadband cavity enhanced absorption spectrometer', *Atmospheric Chemistry and Physics*, 8(24), pp. 7779–7793. doi: 10.5194/acp-8-7779-2008.

Webb, E. K., Pearman, G. I. and Leuning, R. (1980) 'Correction of flux measurements for density effects due to heat and water vapour transfer', *Quarterly Journal of the Royal Meteorological Society*, 106(447), pp. 85–100. doi: 10.1002/qj.49710644707.

Wesely, M. L. (1989) 'Parameterization of surface resistances to gaseous dry deposition in regional-scale numerical models', *Atmospheric Environment (1967)*, 23(6), pp. 1293–1304. doi: 10.1016/0004-6981(89)90153-4.

Wesely, M. L. and Hicks, B. B. (2000) 'A review of the current status of knowledge on dry deposition', *Atmospheric Environment*, 34(12–14), pp. 2261–2282. doi: 10.1016/S1352-2310(99)00467-7.

Wolfe, G. M. *et al.* (2018) 'The NASA Carbon Airborne Flux Experiment (CARAFE): instrumentation and methodology', *Atmospheric Measurement Techniques*, 11(3), pp. 1757–1776. doi: 10.5194/amt-11-1757-2018.

Young, P. J. *et al.* (2018) 'Tropospheric Ozone Assessment Report: Assessment of global-scale model performance for global and regional ozone distributions, variability, and trends', *Elementa*, 6(1), p. 10. doi: 10.1525/elementa.265.

Table 1: Summary of ROZE performance capabilities.

Specification	Value
Size	58 x 44 x 18 ~~cm~~cm^3
Weight	19 kg
Power	< 200 W
Data rate	10 Hz
Precision (1σ, 1Hz)	6.7 x 10^8 ~~molec.~~molecules cm^{-3}
Accuracy	6.2%
Time response	50 ms
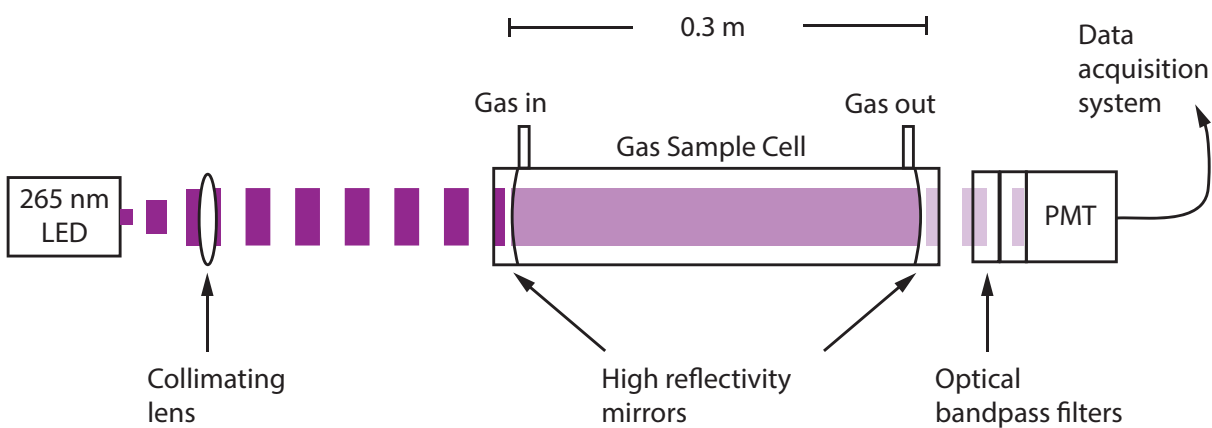
Figure 1: Incoherent broadband cavity enhanced detection technique for O₃. A LED at 265 nm is collimated <u>with a lens</u> and coupled into the detection cell via high reflectivity mirrors (R > 99.7~~%), creating~~<u>%) that comprise the optical cavity and create</u> a long <u>effective</u> optical pathlength. The light attenuated by the sample is then detected using a photomultiplier tube (PMT) operated in analog mode. The sample enters and exits the cell orthogonal to the beam propagation.
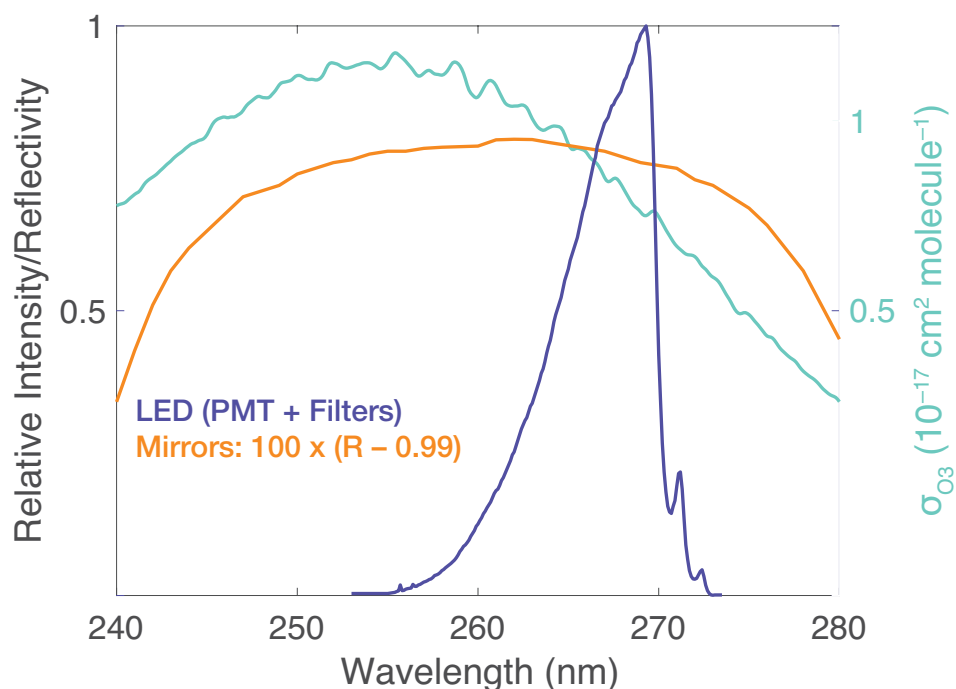
435

13

Figure 2: LED spectrum, mirror reflectivity, and O₃ absorption cross section: The LED (λ_{max} = 265 nm, FWHM = 10 nm) spectrum was measured using a grating spectrometer (0.1 nm resolution) with the instrument PMT and associated detector optics. The mirror curve depicts $100 \times [R - 0.99]$, where R is the reflectivity, over a range of wavelengths. The right axis shows the absorption cross section for the O₃ Hartley band. O₃ and Rayleigh cross sections were determined as the weighted average with the normalized intensity of the LED and PMT detector optics.
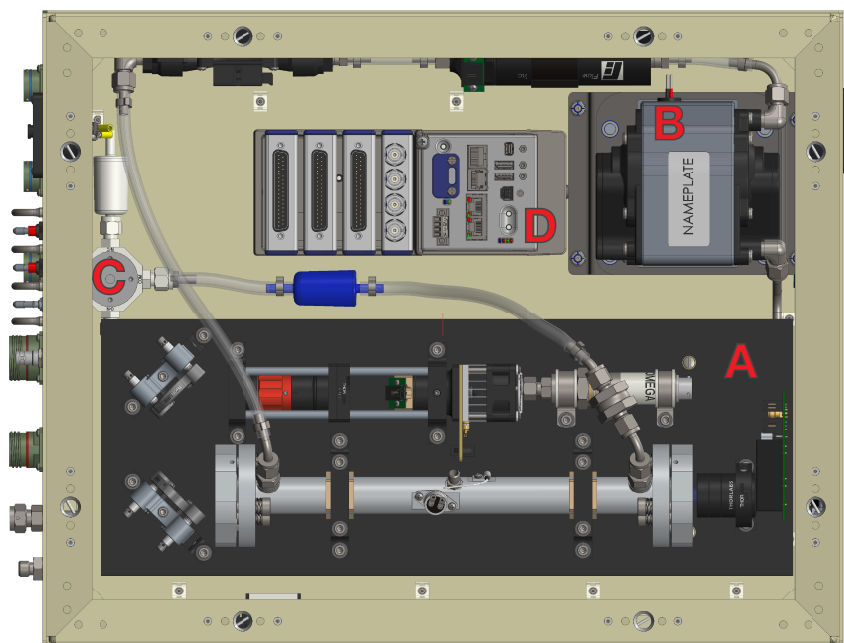
Figure 3: A top view of the ROZE instrument chassis. Major components include A) the optical plate, which consists of the LED assembly, associated optics, the optical cell, and PMT detector; B) The diaphragm pump which can pull up to ~18 SLM through the flow system; C) The 3-way valve which switches between the sample line and air scrubbed of O_3 using a Carulite filter; and D) The data acquisition system.
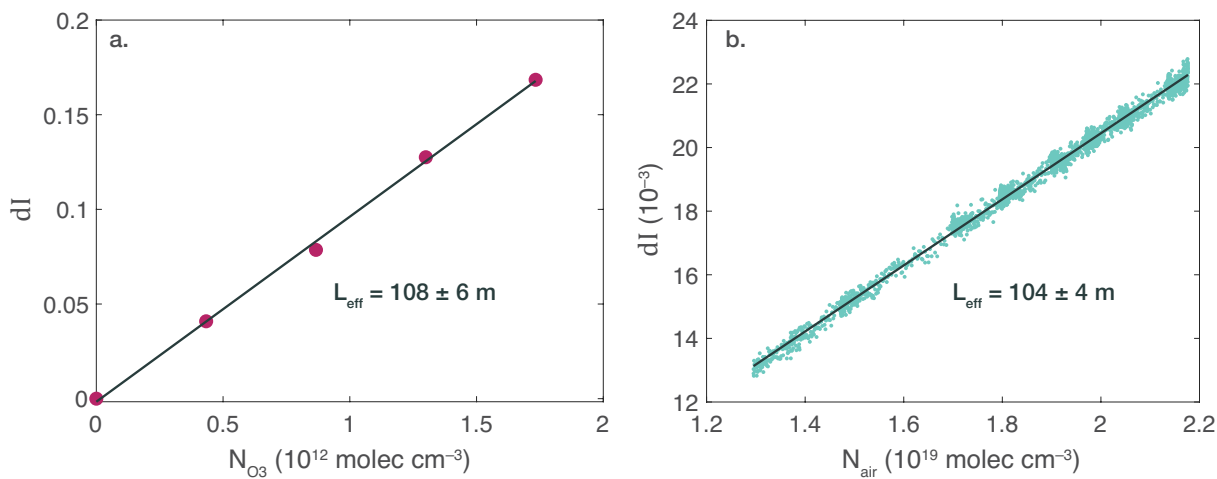
Figure 4: ROZE calibration: a) The effective pathlength (L_{eff}) as determined by attenuation (dI) due to known additions of O$_3$ from a commercial ozone-generator. The slope yields the effective pathlength as determined from Equation 1 in the text using the known O$_3$ absorption cross section; b) Attenuation due to Rayleigh scatter over a range of cell pressures. The slope of attenuation as a function of number density gives the pathlength using the known Rayleigh scattering cross section for zero air. The pathlength derived from both calibrations agrees to within the fit uncertainty.
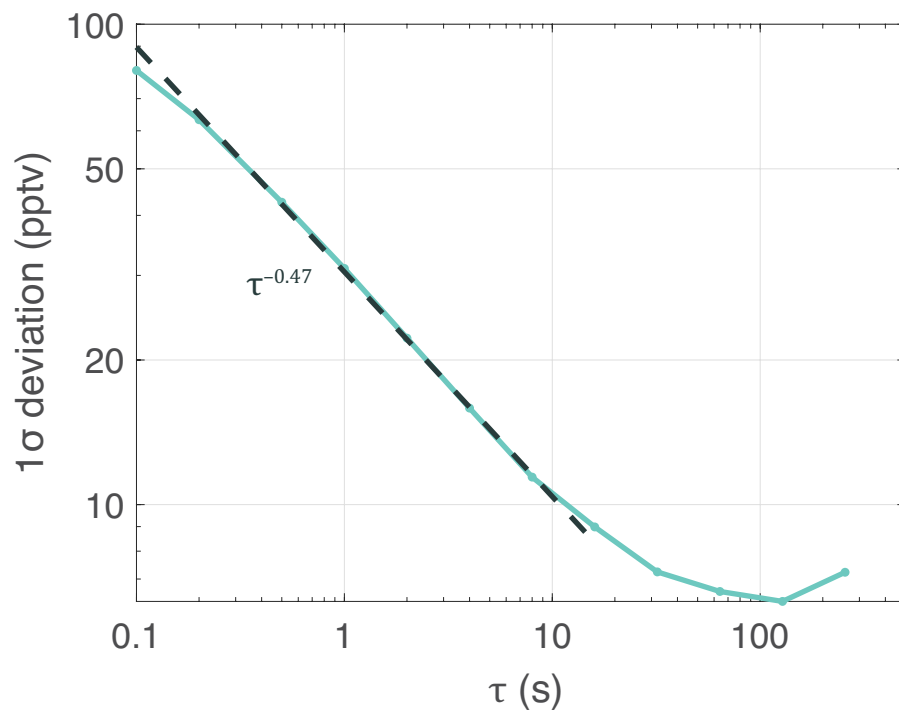
Figure 5: Allan deviation plot for 1.5 hr of sampling zero air at constant pressure (944 mbar). The 1σ precision is expressed in pptv equivalents of O_3 as a function of the integration time τ. The curve demonstrates a precision of 31 pptv in a 1 s integration time. The dashed line shows a $\tau^{-0.47}$ decay for short integration times (< 10 s), comparable to the $\tau^{-1/2}$ decay expected for white noise.
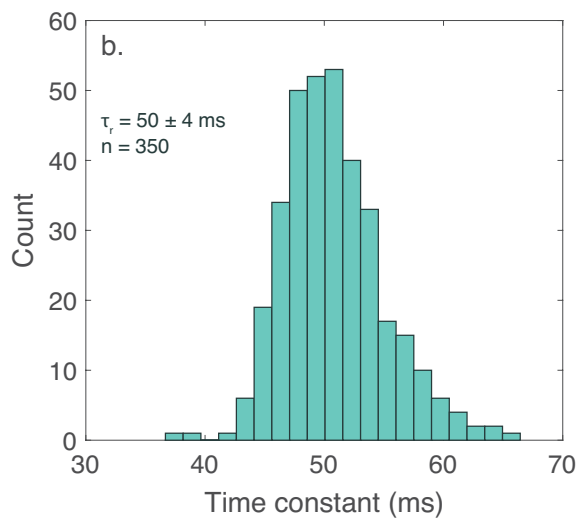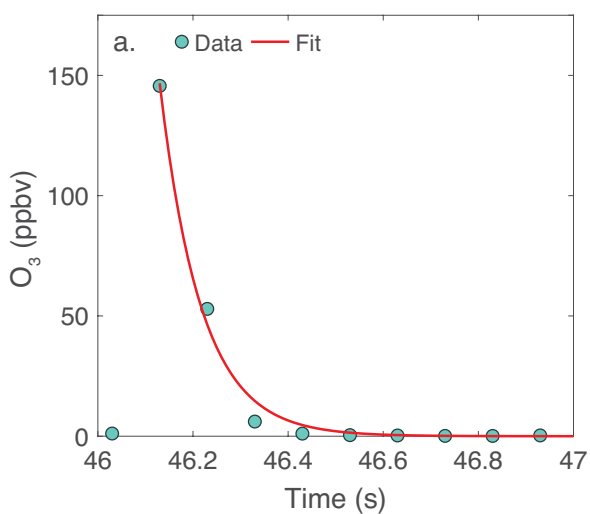
470

475

Figure 6: ROZE time response: a) Ozone was injected into the flow system via a pulsed valve at 2-second intervals with a sample flow of 18 SLM. ~~Individual pulses were fit to~~ An exponential decay ~~using the selected~~function was fitted to each individual pulse (pulse data shown in blue; fit in red); b) Histogram of time constants for all 350 pulses. The *e*-folding decay time of 50 ± 4 ms corresponds to a cell flush rate (1/3e) of 9.5 Hz.

480

18
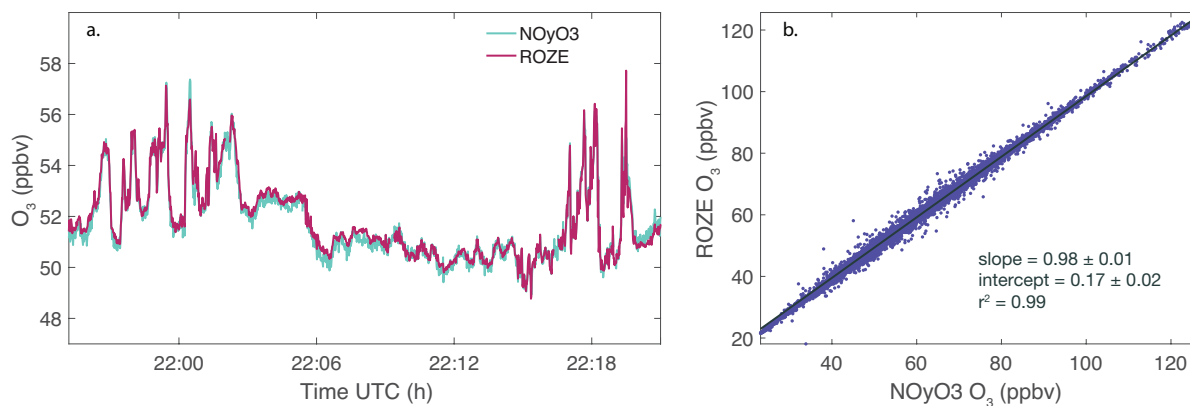
485

Figure 7: ROZE and NOyO3 measurements of O₃ from a FIREX-AQ flight on July 30, 2019 over the Northwestern US: a) Timeseries of ROZE and NOyO3 data (averaged to 1 s); b) ~~Scatter~~Correlation plot of ROZE and NOyO3 O₃ measurements from the full flight. A linear fit to the data yields a slope of 0.98 ± .01 and an intercept of 0.17 ± 0.02 ppbv.
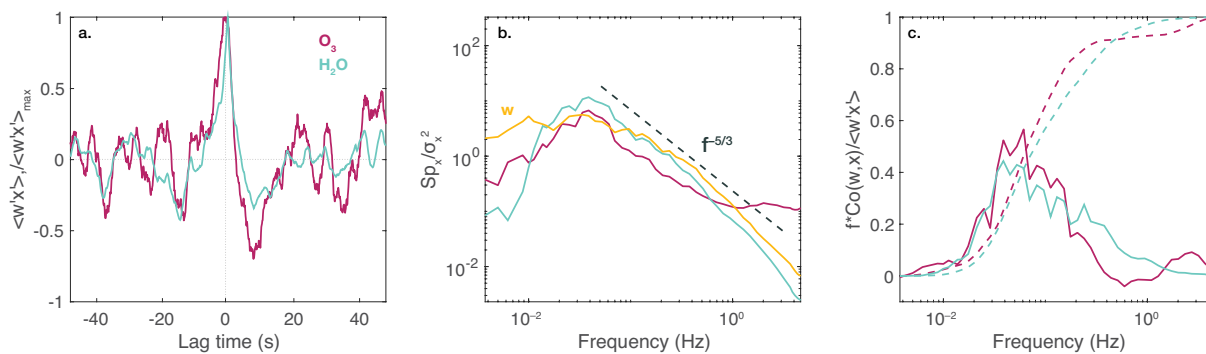
Figure 8: Example spectra from a 50 km flux leg at 170 m altitude during the July 17, 2019 flight over the Pacific Ocean: a) Vertical wind-scalar (w and x respectively) cross covariance functions normalized by the maximum covariance for O_3 and water vapor; b) Power spectra normalized to total variance for w, O_3, and H_2O. The dashed line represents the $f^{-5/3}$ theoretical decay for the inertial subrange; c) Solid lines depict co-spectral power (frequency-multiplied and covariance-normalized) of O_3 and H_2O with vertical wind. Dashed lines depict the respective ogives (cumulative integrals).